Proceedings of 2023 IEEE
International Conference on Mechatronics and Automation
August 6 - 9, Harbin, Heilongjiang, China

A Novel Steerable Catheter for Vascular Interventional Surgery

Yonggan Yan[1], Shuxiang Guo[1,2], Chuqiao Lyu[1], Duohao Zhao[1], Zhijun Lin[1]*

[1] *Key Laboratory of Convergence Biomedical Engineering System and Healthcare Technology, The Ministry of Industry and Information Technology, Beijing Institute of Technology, Beijing, 100081, China*
[2] *The Department of Electronic and Electrical Engineering, Southern University of Science and Technology, Shenzhen, Guangdong 518055,China*
E-mails: {yanyonggan & guoshuxiang}@bit.edu.cn;
*corresponding author

***Abstract*—To improve the operation success rate, the steerable catheter is theoretically significant and practically valuable to design. However, it is still difficult for most existing catheters to realize this function. In this paper, to steer the catheter head, a novel spring-based tendon-drive structure was proposed with a diameter of 1.5mm. To obtain precise tip poses, based on the local force analysis, it is demonstrated that the contact force at each point between the tendon and spring is equal. And under the premise of frictionless, the curvature at each point of the tendon is equal, which is only related to the tension of the tendon. Then the proposed structure is simplified to a cantilever beam only subjected to bending moment. And the deformation of the catheter tip with the control parameters is expressed. Finally, the experimental setup is established and the experimental results showed that the proposed spring-based tendon-driven catheter deflected in a circular. And the results justified the feasibility of the cantilever beam assumption and the correctness of the deformation formulas. The proposed tendon-driven catheter has the potential in improving the success rate of the vascular approach and operation safety.**

Index Terms*—Steerable catheter, vascular interventional surgery robot, tendon-driven, active bending.

I. Introduction

Cardiovascular and cerebrovascular diseases, which have become the diseases with the highest morbidity and mortality except infectious diseases, are the number one killer of human beings [1]. It mainly includes arterial stenosis, cerebral aneurysm, and so on. Traditional treatment methods include craniotomy, thoracotomy, and minimally invasive interventional surgery. The former will cause greater trauma and pain, while the latter has almost no trauma and discomfort. Therefore, the latter has become the main treatment for these diseases [2]. It is usually punctured in the femoral artery or radial artery, and the path from the puncture port to the affected area is established with the help of thin catheters, guidewires, and other instruments. Then, depending on the type and extent of the disease, surgery such as artery stenosis percutaneous transluminal angioplasty, or endovascular embolization in intracranial aneurysms is performed. To obtain the real-time position of the catheter and guidewire in the body, the surgeons use the Digital Subtraction Angiography System(DSA system) to visualize the blood vessels. During this process, the system will generate radiation, which causes cumulative damage to surgeons [3]–[6]. The master-slave surgery robot, which can isolate surgeons and patients, solves this problem, and the control framework is shown in Fig. 1. The master manipulator collects the effective operation information of surgeons outside the operating room and transmits it to the slave side robot in the operating room. Based on the surgeons' motion signal, the slave side robot operates the surgical instruments. The force-position information in the operation is collected by the slave side robot and fed back to the surgeon, which is used for decision-making of the operation states [7]–[11].

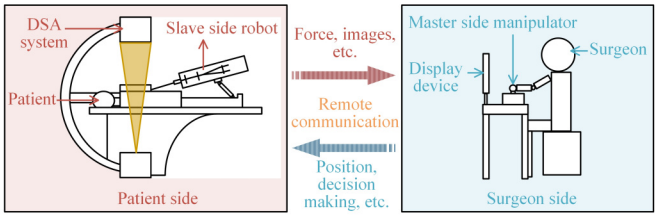

Fig. 1. Control framework of the master-slave VIS robot.

Almost the existing catheters and guidewires are passively flexible, which are highly redundant and difficult to control the tip pose. The flexible catheters and guidewires can complete the blood vessel approach after being shaped by surgeons, which requires rich surgical experience and skilled operation skills. Therefore, developing a steerable catheter with an active bending tip can improve the success rate of the blood vessel approach and decrease the contact force between the blood vessel and catheter tip [12]. So far, there are three main methods to realize the steerable catheter tip, including the tendon-driven catheter [13], Shape memory alloy actuated

979-8-3503-2084-8/23/$31.00 ©2023 IEEE

devices [14], and magnetically actuated catheters or wires [15]–[17]. Among them, the tendon-driven steerable catheter is a simple control, precise, and low-cost method. It should be noted that the tendon-driven catheter tip can bend over 180°, which is important for the tortuous blood vessel. David B et al. proposed a mechanics modeling method for tendon-driven continuum manipulators. The single tendon-driven catheter was modeled as a cantilever beam, and the simplified model was justified by theoretical derivation and experiments [18]. Yash et al. designed a 2-degree-of-freedom steerable guidewire laser micro-machined and proposed a tendon-driven method [13]. Nancy J. et al. designed a tendon-driven catheter tip. The catheter system can predict and reconstruct the deformation and contact force of the catheter tip by a triplet of adhered single core fiber Bragg grating sensors [12]. Generally speaking, the steerable catheter and guidewire are a valuable direction. On the one hand, the active bending tip can improve the success rate of the blood vessel approach and decrease the difficulty of surgery. On the other hand, it can reduce the workload of surgeons and the radiation damage to the body.

The major objective of this paper is to develop a tendon-driven catheter with precise pose control. To this aim, a spring-based single-tendon-driven structure is designed. The deformation features of the catheter active section are analyzed. And the relationship between the deformation of the active section and displacement of the tendon is obtained. Finally, the active deformation catheter experimental setup is established to verify the feasibility of the proposed catheter structure and the efficiency of the theory.

II. Structure Design

In this section, a spring-based tendon-driven steerable catheter is designed to satisfy the tip-bending function. Firstly, a spring-based tendon-driven structure is proposed as shown in Fig. 2. Then the kinematics of the structure is calculated to obtain the relationship between the bending deformation and the tendon displacement. Secondly, the actuator unit structure of the tendon-driven mechanism is designed, and a closed-loop control system is built to realize precise control.

A. Spring-based Tendon-driven Catheter Mechanical Design

To suit the various blood environment and improve the success rate of the surgery approach, the catheter tip usually is designed in various shapes, such as the pigtail catheter, Headhunter catheter, Simmon catheter, and so on. Although the existing catheters can meet most situations, surgeons still often shape the catheter tip manually due to the complex and individualized blood environment, even multiple shaping the catheter tip in the same area. The active bendable catheter solves the problem and greatly improves the success rate of the blood vessel approach and efficiency. As shown in Fig. 2, a spring-based tendon-driven catheter tip structure is designed. It mainly consists of a support spring, a stainless steel spine, a tendon, and a silicone coating. The active bendable catheter solves the problem and greatly improves the success rate of the blood vessel approach and efficiency. As shown in Fig. 2, a spring-based tendon-driven catheter tip structure is designed. It mainly consists of the active section and passive section, as shown in the red background area and blue background area, respectively. The active section mainly includes a support spring, a stainless steel spine, a tendon, and a silicone coating. The stainless steel spine is fixed with each turn of the support spring. The length of the spine is equal to the original length of the spring, so the original state of the spring is straight. One end of the tendon is fixed with the end of the spring, and another end is connected with the actuator unit. The bending of the tip of the catheter can be realized by pulling the tendon. And the rebound relies on the elasticity of the spine and releasing the tendon. The passive section is lined with PTFE pipe, which has the characteristics of smooth surface and flexibility. And the surface of the catheter is covered with a polyurethane hydrophilic coating to reduce friction with the vessel wall.

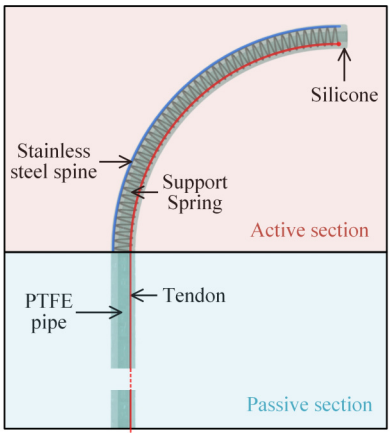

Fig. 2. Stucture of the proposed bendable catheter.

The 2D structure diagram of the bending catheter tip is shown in Fig. 3. Because the spine is fixed with each turn of the support spring, the spring will bend to another side of the non-fixed side of the spring with the pulling of the tendon. Next, we will demonstrate that the active section will bend in a circular arc without considering the friction between the spring and the tendon. As shown by the red lines in Fig. 3(b), a section between the adjacent contact points of the support spring and the tendon is intercepted, and its force analysis is carried out. It is known that the pulling force of the tendon is T, and the force direction is tangent to the ends of the intercepted segment, respectively, that is, $T_i = T_{i+1} = T$. The ends of the intercepted spine are subject to the contact force of spring, and the forces' directions are along with the radial direction of the circular near the contact points,

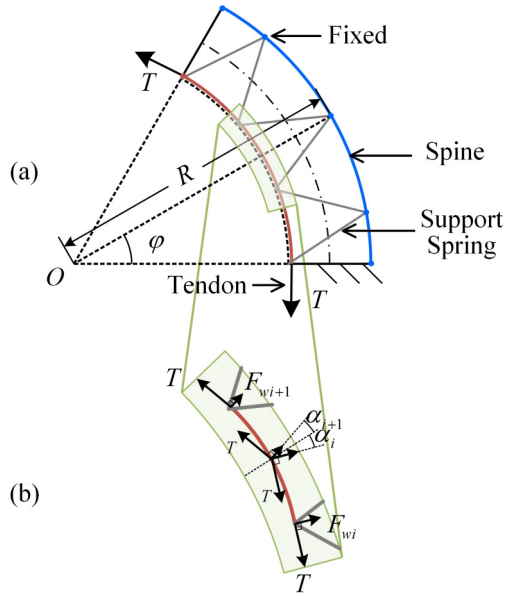

Fig. 3. Catheter manipulating diagram. (a) A section of the catheter tip is deflected by the tendon. (b) Force analysis of a tendon segment.

respectively. The contact force between the tendon and the i_{th} turn of spring is F_{wi}, and the contact force between the tendon and the $i+1_{th}$ turn of spring is F_{wi+1}. It is assumed that the two contact force is different, for example, $F_{wi} > F_{wi+1}$, as shown in Fig. 3(b). Then the forces of two ends are translated to the center of the intercepted tendon, and draw the bisector of the T_i and T_{i+1}. Due to the radial force F_{wi}, F_{wi+1} are perpendicular to T_i, T_{i+1}, respectively, the angles between two contact forces and the angle bisector are equal, that is, $\alpha_i = \alpha_{i+1}$. The static equilibrium analysis is performed on the vertical line of the angle bisector, which can be expressed as:

$$\begin{bmatrix} F_{wi} & T_i \end{bmatrix} \begin{bmatrix} \sin\alpha_i \\ \cos\alpha_i \end{bmatrix} = \begin{bmatrix} F_{wi+1} & T_{i+1} \end{bmatrix} \begin{bmatrix} \sin\alpha_{i+1} \\ \cos\alpha_{i+1} \end{bmatrix} \quad (1)$$

that is:

$$F_{wi} = F_{wi+1} \quad (2)$$

In the same way, the conclusion is extended to each node, and the contact force at each contact point between the tendon and the support spring is equal.

Taking the micro section of the tendon near the contact point is shown in Fig. 4. It is assumed that the micro section is a circular arc with the length $\mathrm{d}s_i$, deflection angle $\mathrm{d}\varphi_i$, transverse force $\mathrm{d}F_{wi}$, tension force T. The static equilibrium analysis on microelements is performed as shown in Fig. 4 and can be expressed as:

$$\mathrm{d}F_{wi} = 2T \cdot \sin(\frac{\mathrm{d}\varphi_i}{2}) \quad (3)$$

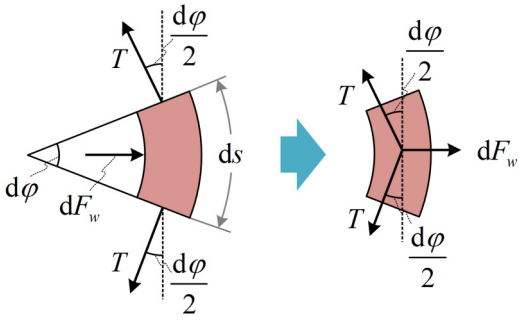

Fig. 4. Force analysis of a tendon element.

Take the limit of $\sin(\frac{\mathrm{d}\varphi}{2})$ and can be expressed as:

$$\mathrm{d}F_{wi} = T \cdot \mathrm{d}\varphi_i \quad (4)$$

Both ends of (4) are divided by $\mathrm{d}s_i$ and is expressed as:

$$\frac{\mathrm{d}F_{wi}}{\mathrm{d}s_i} = T \cdot \frac{\mathrm{d}\varphi_i}{\mathrm{d}s_i} = T \cdot \kappa_i \quad (5)$$

where κ_i represents the curvature of the microelement, $\mathrm{d}s_i$ represents the arc length of the microelement, which is a minimal constant. Formula (5) shows that the transverse force $\mathrm{d}F_{wi}$ is only related to the tension force T and the microelement curvature κ_i. Based on formula (2), the contact forces between the tendon and each turn of the support spring are equal. Therefore, the curvature of each contact point is equal without considering the friction, that is:

$$\kappa_1 = \kappa_i = c \quad (6)$$

where c is a constant. Therefore, when the number of the turn of the spring is sufficient, we can approximate that the proposed tendon-driven structure bends in a circular arc without considering friction.

B. Deformation Analysis of Catheter Active Part

The deformation of the catheter active section is analyzed further, and the force on the active section is shown in Fig. 5(a). The active section is considered a unit, so the contact forces between the spring, the tendon, and the spine are internal, which can be ignored. Therefore, the active section is under the pulling force of the tendon and a bending moment due to the interval between the tendon and the spine. The moment can be expressed as:

$$M = T \cdot d \quad (7)$$

where M represents the bending moment, d represents the force arm. With the support of the spine, the deformation caused by the axial tension can be ignored. Therefore, the active section is simplified to a cantilever beam only under the bending moment, as shown in Fig. 5(b). The Bernoulli-Euler equation can be written as:

$$\frac{\mathrm{d}\theta}{\mathrm{d}s} = \frac{M}{EI} \quad (8)$$

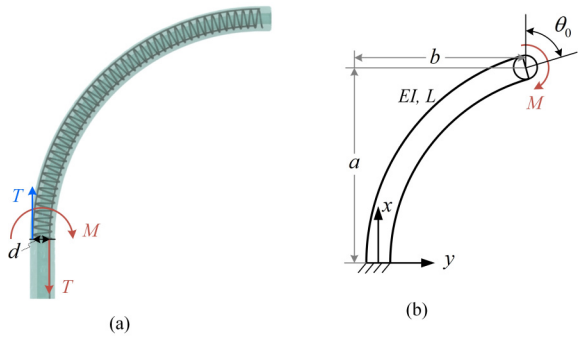

Fig. 5. Deformation analysis of the catheter active section. (a) Force on the active section. (b) Equivalent simplified model.

where M is a constant along the beam. The deformation angle θ_0 of the beam end can be calculated by separating variables and integrating:

$$\int^{\theta_0} \mathrm{d}\theta = \int_0^L \frac{M}{EI}\mathrm{d}s \tag{9}$$

$$\theta_0 = \frac{ML}{EI} \tag{10}$$

The formula (9) doesn't have the small deformation hypothesis because it is the integral of the distance s along the beam direction rather than x.

The deformation in the vertical direction can be calculated by differential chain rule:

$$\frac{M}{EI} = \frac{\mathrm{d}\theta}{\mathrm{d}s} = \frac{\mathrm{d}\theta}{\mathrm{d}y}\frac{\mathrm{d}y}{\mathrm{d}s} \tag{11}$$

Due to $\frac{\mathrm{d}y}{\mathrm{d}s} = \sin\theta$, the formula (10) can be expressed as:

$$\frac{M}{EI} = \frac{\mathrm{d}\theta}{\mathrm{d}y} \cdot \sin\theta \tag{12}$$

Separate the variables and integrate (12):

$$\int_0^b \mathrm{d}y = \frac{M}{EI}\int_0^{\theta_0} \sin\theta \mathrm{d}\theta \tag{13}$$

$$b = \frac{EI}{M}(-cos\theta_0 + 1) \tag{14}$$

Substituting (10) into (14):

$$b = \frac{1 - cos\theta_0}{\theta_0} \cdot L \tag{15}$$

Similarly, the deformation in level can be obtained. The Bernoulli-Euler equation can be written as:

$$\frac{M}{EI} = \frac{\mathrm{d}\theta}{\mathrm{d}s} = \frac{\mathrm{d}\theta}{\mathrm{d}x}\frac{\mathrm{d}x}{\mathrm{d}s} \tag{16}$$

Due to $\frac{\mathrm{d}x}{\mathrm{d}s} = cos\theta$, (16) can be written as:

$$\frac{M}{EI} = \frac{\mathrm{d}\theta}{\mathrm{d}x} \cdot \cos\theta \tag{17}$$

TABLE I
ORTHOGONAL FORCE COUPLED MODEL FITTING PARAMETERS FOR CATHETER AND GUIDEWIRE

Parameters	Value
Spine length (mm)	20
Spine diameter(mm)	0.1
spring diameter(mm)	1
Spring minor diameter(mm)	0.15
Active section diameter(mm)	1.5

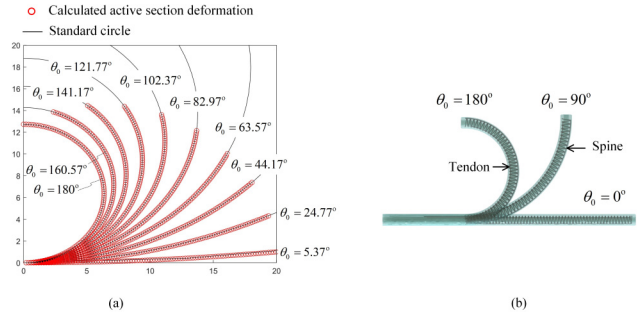

Fig. 6. Calculation of deformation trajectories of the active section. (a) Deformation trajectories of the active section. (b) Deformation of the active section.

Separate variables and integrate (17):

$$\int_0^a \mathrm{d}x = \frac{M}{EI}\int_0^{\theta_0} \cos\theta \mathrm{d}\theta \tag{18}$$

$$a = \frac{\sin\theta_0}{\theta_0} \cdot L \tag{19}$$

The parameters of the active section are shown in TABLE I.

The active section is divided into 100 equal parts along the axis direction. Substitute the parameters of TABLE I into formulas (15) and (19) and draw the deformation trajectories of the 100 points in different deformation angles of the cantilever beam, as shown in Fig. 6(a). The red circles represent the calculated points of the active section and the black lines represent standard circles. As shown in Fig. 6(a), the calculated points coincide with the standard circle at a deformation angle. It is indicated that the active section, after simplified as a cantilever beam only under the bending moment, deformation trajectories are circular, which is coincident with the conclusion of $Section(A)$ without considering friction. Therefore, without considering the friction between the tendon and the support spring, the active section can be simplified as a cantilever beam only under the bending moment.

In the following the relationship between the deformation of the active section and the control parameter, that is, the displacement of the tendon is calculated. The active section state with the tendon displacement Δp is shown in Fig. 7. O

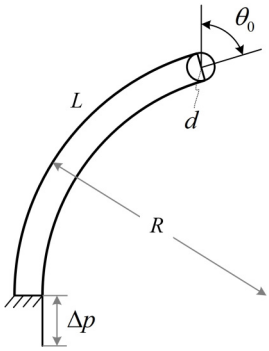

Fig. 7. Relationship between the displacement of the tendon and the deformation of the active section.

represents the circle center of the active section, r represents the bending inner radius, and R represents the outer radius. The inner circle arc length L' can be written as:

$$L' = \int_0^{\theta_0} (R - d)\mathrm{d}\theta \tag{20}$$

L' also can be expressed as:

$$L' = L - \Delta p \tag{21}$$

$Deltap$ Can be written as:

$$\Delta p = \int_0^{\theta_0} R\mathrm{d}\theta - \int_0^{\theta_0} R\mathrm{d}\theta + \int_0^{\theta_0} d\mathrm{d}\theta \tag{22}$$

Integrate (22) and obtain the deformation angle θ_0:

$$\theta_0 = \frac{\Delta p}{d} \tag{23}$$

The bending radius can be written as:

$$R = \frac{L}{\theta_0} = \frac{L \cdot d}{\Delta p} \tag{24}$$

III. Evaluation and Experiments

In this section, series experiments were performed to verify the proposed structure and methods, including the circular deformation of the active section, the relationship between the displacement of the tendon and the deformation, and the stability of the active section.

The experimental setup was established to measure the deformation of the active section, including the active section of the catheter, the tendon, a Y-type valve, a Maxon motor, a camera, and a square grid. The active section threaded into the Y-type valve, and the tendon was actuated by a Maxon motor with a rack and pinion mechanism. The displacement of the tendon was calculated by the encoder of the motor:

$$\Delta p = \theta_m \cdot r_g \tag{25}$$

where θ_m represents the rotation angle of the motor, and r_g represents the radius of the indexing circle of the rack.

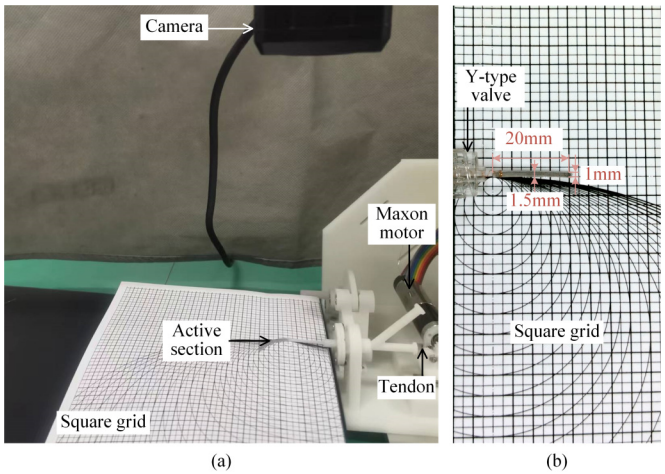

Fig. 8. Experimental setup. (a) Experimental setup structure. (b) Deformation measurement scheme.

To verify the active section bending in a circle arc without considering the friction, the contour of the active section was compared to the square grid, as shown in Fig. 8(b). The grid was drawn with a series of circles with different diameters, and these circles have the same inner tangent point and a radius resolution of 2.5mm. The root of the active section was fixed in the tangent point, and then the tendon was pulled by the motor. The deformation trajectory was collected by the camera. It should be noted that a vibration-pulling method was adopted to release the friction between the tendon and spring, and reduce the influence of friction.

In the experiment, the deformation state was controlled by the displacement of the tendon, and aligned with the different standard circles. The position of the end of the active section, the deformation angle, and the tendon displacement were recorded. The experimental results were shown in Fig. 9. The comparison between the active section contour and standard circles showed that the spine can align with the standard circles. It is indicated that the proposed spring-based tendon-driven catheter bends in circular arcs without considering friction.

The curve between the bending radius and the real displacement of the tendon was shown in the red triangle of Fig. 10. The curve between the bending radius and the calculated displacement of the tendon was shown in the blue five-pointed stars and blue lines of Fig. 10. The results showed that the calculated curve was coincident with the real curve. The mean absolute error was 0.109mm, and the relative error is 6.53%. It showed the efficiency of the theory analysis and formulas.

IV. Conclusion

In this paper, a novel tendon-driven catheter was proposed to realize the active bending of the tip. To this aim, a

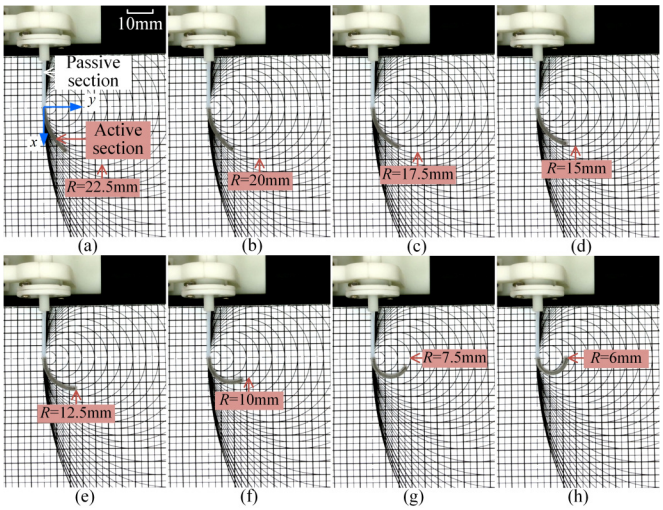

Fig. 9. Experimental results of the active section deformation. (a) R=22.5mm. (b) R=20mm. (c) R=17.5mm. (d) R=15mm. (e) R=12.5mm. (f) R=10mm. (g) R=7.5mm. (h) R=6mm.

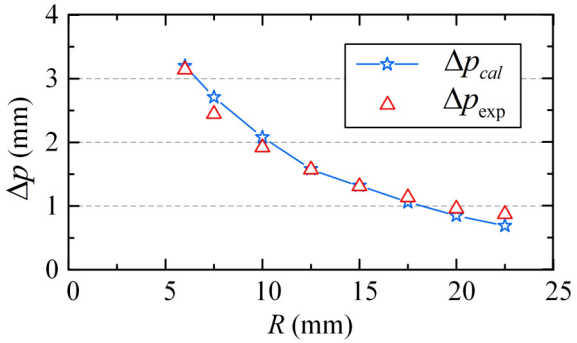

Fig. 10. Experimental results.

spring-based tendon-driven structure was designed. Firstly, it was demonstrated that the contact forces of the tendon contact points with the support spring were equal. Then the conclusion, the curvature on each contact point of the tendon was equal, was obtained without considering friction. To obtain the relationship between the deformation of the active section and the displacement of the tendon, the active section was simplified to a cantilever beam, and the expressions for the deformation features of the active section were calculated. Finally, the experimental setup for the evaluation of the proposed catheter was established. The experimental results verified that the active section bent in circular arcs without considering friction, and the active section structure can be simplified to a cantilever beam correctly. The proposed steerable catheter has the potential in improving the safety, efficiency, and success rate of the blood vessel approach.

REFERENCES

[1] W. H. Organization, "World health statistics 2021: monitoring health for the sdgs, sustainable development goals," World Health Organization, Tech. Rep., 2020.

[2] A. Hooshiar, A. Payami, J. Dargahi, and S. Najarian, "Magnetostriction-based force feedback for robot-assisted cardiovascular surgery using smart magnetorheological elastomers," *Mech Syst Signal Pr*, vol. 161, p. 107918, 2021.

[3] L. W. Klein and E. P. Campos, "Occupational hazards in the cath lab-physician, protect thyself!" *J Invasive Cardiol*, vol. 30, no. 2, pp. 75–76, 2018.

[4] Y. Yan, S. Guo, C. Lyu, D. Zhao, and Z. Lin, "Sea-based humanoid finger-functional parallel gripper with two actuators: Pg2 gripper," *IEEE Transactions on Instrumentation and Measurement*, 2022.

[5] X. Bao, S. Guo, Y. Guo, C. Yang, L. Shi, Y. Li, and Y. Jiang, "Multilevel operation strategy of a vascular interventional robot system for surgical safety in teleoperation," *IEEE Transactions on Robotics*, vol. 38, no. 4, pp. 2238–2250, 2022.

[6] P. Shi, S. Guo, L. Zhang, X. Jin, H. Hirata, T. Tamiya, and M. Kawanishi, "Design and evaluation of a haptic robot-assisted catheter operating system with collision protection function," *IEEE Sensors Journal*, vol. 21, no. 18, pp. 20 807–20 816, 2021.

[7] C. Lyu, S. Guo, W. Zhou, Y. Yan, C. Yang, Y. Wang, and F. Meng, "A deep-learning-based guidewire compliant control method for the endovascular surgery robot," *Micromachines*, vol. 13, no. 12, p. 2237, 2022.

[8] Y. Yan, H. Wang, H. Yu, F. Wang, J. Fang, J. Niu, and S. Guo, "Machine learning-based surgical state perception and collaborative control for a vascular interventional robot," *IEEE SENS J*, vol. 22, no. 7, pp. 7106–7118, 2022.

[9] X. Li, S. Guo, P. Shi, X. Jin, M. Kawanishi, and K. Suzuki, "A bimodal detection-based tremor suppression system for vascular interventional surgery robots," *IEEE Transactions on Instrumentation and Measurement*, vol. 71, pp. 1–12, 2022.

[10] X. Jin, S. Guo, J. Guo, P. Shi, M. Kawanishi, and H. Hirata, "Active suppression method of dangerous behaviors for robot-assisted vascular interventional surgery," *IEEE Transactions on Instrumentation and Measurement*, vol. 71, pp. 1–9, 2022.

[11] W. Zhou, S. Guo, J. Guo, F. Meng, Z. Chen, and C. Lyu, "A surgeon's habits-based novel master manipulator for the vascular interventional surgical master-slave robotic system," *IEEE Sensors Journal*, vol. 22, no. 10, pp. 9922–9931, 2022.

[12] N. J. Deaton, T. A. Brumfiel, A. Sarma, and J. P. Desai, "Simultaneous shape and tip force sensing for the coast guidewire robot," *IEEE Robotics and Automation Letters*, 2023.

[13] Y. Chitalia, X. Wang, and J. P. Desai, "Design, modeling and control of a 2-dof robotic guidewire," in *2018 IEEE International Conference on Robotics and Automation (ICRA)*. IEEE, 2018, pp. 32–37.

[14] A. T. Tung, B.-H. Park, G. Niemeyer, and D. H. Liang, "Laser-machined shape memory alloy actuators for active catheters," *IEEE/ASME transactions on mechatronics*, vol. 12, no. 4, pp. 439–446, 2007.

[15] J. Kim, P. B. Nguyen, B. Kang, E. Choi, J.-O. Park, and C.-S. Kim, "A novel tip-positioning control of a magnetically steerable guidewire in sharply curved blood vessel for percutaneous coronary intervention," *International Journal of Control, Automation and Systems*, vol. 17, no. 8, pp. 2069–2082, 2019.

[16] D. Liu, X. Liu, Z. Chen, Z. Zuo, X. Tang, Q. Huang, and T. Arai, "Magnetically driven soft continuum microrobot for intravascular operations in microscale," *Cyborg and Bionic Systems*, vol. 2022, 2022.

[17] S. Zhang, M. Yin, Z. Lai, C. Huang, C. Wang, W. Shang, X. Wu, Y. Zhang, and T. Xu, "Design and characteristics of 3d magnetically steerable guidewire system for minimally invasive surgery," *IEEE Robotics and Automation Letters*, vol. 7, no. 2, pp. 4040–4046, 2022.

[18] D. B. Camarillo, C. F. Milne, C. R. Carlson, M. R. Zinn, and J. K. Salisbury, "Mechanics modeling of tendon-driven continuum manipulators," *IEEE Transactions on Robotics*, vol. 24, no. 6, pp. 1262–1273, 2008.